

VILNIUS UNIVERSITY
CENTER FOR PHYSICAL SCIENCES AND TECHNOLOGY
INSTITUTE OF PHYSICS

Marijus Brikas

**MICROPROCESSING OF SILICON AND METALS
WITH HIGH-PULSE-REPETITION-RATE
PICOSECOND LASERS**

Summary of doctoral thesis
Technological sciences, Material engineering (08 T),
Laser technology (T 165)

Vilnius, 2011

Dissertation was prepared in 2005 – 2009 at Institute of Physics of the Center for Physical Sciences and Technology (CPST)

Scientific supervisor:

Dr. Gediminas Račiukaitis (Institute of Physics, CPST, technological sciences, material engineering – 08T, laser technologies – T165)

Doctoral thesis will be defended at the Center for Physical Sciences and Technology in the senate of Material engineering:

Chairman:

Prof. habil. Dr. Valerijus Smilgevičius (Vilnius University, technological sciences, material engineering – 08T, laser technologies – T165)

Members:

1. Prof. habil. Dr. Arūnas Krotkus (Semiconductor physics institute, CPST, technological sciences, material engineering – 08T, laser technologies – T165)
2. Prof. habil. Dr. Eugenijus Šatkovskis (Vilnius Gediminas Technical University, technological sciences, material engineering – 08T, laser technologies – T165)
3. Prof. habil. Dr. Rimantas Vaišnoras (Vilnius Pedagogical University, physical sciences, physics – 02P)
4. Dr. Irmantas Kašalynas (Semiconductor physics institute, CPST, physical sciences, physics – 02P)

Official opponents:

1. Prof. habil. Dr. Sigitas Tamulevičius (Kaunas University of Technology, technological sciences, material engineering – 08T, material technology – T150)
2. Dr. Raimondas Petruškevičius (Institute of Physics, CPST, technological sciences, material engineering, laser technologies – T165)

This thesis will be under open consideration on the 23rd of March, 2011 3 p.m. at the Hall of CPST Institute of physics.

Adress: Savanorių ave. 231, LT-02300 Vilnius, Lietuva.

Summary of doctoral thesis has been distributed on 22 of February, 2011.

Doctoral thesis is available at libraries of CPST and Vilnius University.

VILNIAUS UNIVERSITETAS
FIZINIŲ IR TECHNOLOGIJOS MOKSLŲ CENTRO
FIZIKOS INSTITUTAS

Marijus Brikas

**SILICIO IR METALŲ MIKROAPDIRBIMAS DIDELIO
IMPULSŲ PASIKARTOJIMO DAŽNIO
PIKOSEKUNDINIAIS LAZERIAIS**

Daktaro disertacijos santrauka
Technologijos mokslai, Medžiagų inžinerija (08 T),
Lazerinė technologija (T 165)

Vilnius, 2011

Disertacija rengta 2005 – 2009 metais Fizikos institute

Mokslinis vadovas:

Dr. Gediminas Račiukaitis (FTMC Fizikos institutas, technologijos mokslai, medžiagų inžinerija – 08T, lazerinė technologija – T165)

Disertacija ginama Vilniaus Universiteto Medžiagų inžinerijos krypties taryboje:

Pirmininkas:

Prof. habil. dr. Valerijus Smilgevičius (Vilniaus universitetas, technologijos mokslai, medžiagų inžinerija – 08T, lazerinė technologija – T165)

Nariai:

1. Prof. habil. dr. Arūnas Krotkus (FMTC Puslaidininkių fizikos institutas, technologijos mokslai, medžiagų inžinerija – 08T, lazerinė technologija – T165)
2. Prof. habil. dr. Eugenijus Šatkovskis (Vilniaus Gedimino technikos universitetas, technologijos mokslai, medžiagų inžinerija – 08T, lazerinė technologija – T165)
3. Prof. habil. dr. Rimantas Vaišnoras (Vilniaus pedagoginis universitetas, fiziniai mokslai, fizika – 02P)
4. dr. Irmantas Kašalynas (FMTC Puslaidininkių fizikos institutas, fiziniai mokslai, fizika – 02P)

Oponentai:

1. Prof. habil. dr. Sigitas Tamulevičius (Kauno technologijos universitetas, technologijos mokslai, medžiagų inžinerija – 08T, medžiagų technologija – T150)
2. dr. Raimondas Petruškevičius (FTMC Fizikos institutas, technologijos mokslai, medžiagų inžinerija – 08T, lazerinė technologija – T165)

Disertacija bus ginama viešame Medžiagų inžinerijos krypties tarybos posėdyje 2011m. kovo mėn. 23 d 15 val. FMTC Fizikos instituto salėje.

Adresas: Savanorių pr. 231, LT-02300 Vilnius, Lietuva.

Disertacijos santrauka išsiuntinėta 2011 metų vasario mėn. 22 d..

Disertaciją galima peržiūrėti Vilniaus universiteto ir FMTC bibliotekose.

Contents

Introduction.....	6
Relevance.....	7
The scientific tasks of this work.....	8
Statements to be defended.....	8
Author’s publications, related to thesis.....	9
Summary of doctoral thesis.....	10
Introduction.....	10
Chapter I. Laser radiation properties and interaction with material.....	10
Chapter II. Review of laser microfabrication studies.....	10
Chapter III Methods of laser micromachining analysis.....	10
Chapter IV Ablation with high repetition rate nanosecond and picosecond pulses.....	12
Ablation threshold and accumulation effects.....	12
Ablation rate.....	14
Optimization of laser beam focusing.....	15
Chapter V Microprocessing of silicon with picosecond lasers.....	18
Auger electron spectra.....	22
Chapter VI Applications of high-repetition-rate picosecond lasers in microfabrication	24
Surface roughness and ablation regimes.....	24
Formation of 3D structures in metals.....	25
Laser processing of Nitinol.....	25
Stent cutting using high repetition rate picosecond lasers.....	26
Chapter VII Generation of nanoparticle colloids by picosecond laser ablation in liquid flow.....	27
Conclusions.....	28

Introduction

Laser systems and optical tools for laser-material processing are advancing rapidly on several evolutionary fronts. Both diode-pumped lasers are now firmly entrenched in industrial processing as reliable tool for diverse material processing applications. Compact laser systems offer a wide assortment of wavelengths, pulse durations, and power levels to precisely control laser-matter interactions and provide special capabilities needed for exploiting a much broader base of industrial applications.

New technological needs in various key areas of material processing such as microelectronics, nanoscience or biology have motivated the development of novel alternative techniques which are able to respond to the new technological requests for more precision, higher resolution and better surface and volume localization. Indeed, in addition to the intrinsic properties of lasers, i.e. monochromaticity, spatial and temporal coherence, low divergence and very high power density, are now easily obtained with ultrashort pulses. This represents therefore a powerful tool to induce structural or morphological modifications in the near-surface region of solids, as well as structural ordering and phase transformations of metals [1].

Silicon remains as the most important material for intelligent microscale machines that combine sensors and actuators, mechanical structures and electronics to sense information from the environment and react to it. Pricing and reliability considerations have led to the almost exclusive use of silicon-based micro-mechanical devices [2].

Laser ablation in liquids is attracting much attention as a new technique to prepare nanoparticles. An advantage of this technique is simplicity of the procedure. In principle, nanoparticles of various species of materials can be prepared by using one procedure [3]. Nanoparticles are used in biomedical applications such as antibacterial implants or catheters, modification of textiles, and refinement of polymers. Very often the desired range of applications is restricted due to a limited availability of nanoparticle materials, their purity and their redispersability from agglomerates [4,5]. Although 5–100 nm

nanoparticles can be produced by a relatively simple chemical reduction method, the surface of these nanoparticles is likely to be contaminated with reaction by-products such as anions and reducing agents, which can interfere with subsequent stabilization and functionalization steps [6].

It has been shown that laser ablation in liquid produces surface-charged nanoparticles with a shell of dipole molecules (e.g., water) formed around them and preventing agglomeration [3].

Relevance

The need for metal and silicon laser micromachining turned out when this study started. Up to year 2005, Q-switched lasers, working at repetition rates of several tenths of kilohertz, dominated in laser microfabrication. Mode-locked lasers were working at low pulse repetition rates, usually lower than 1 kHz, and were too slow for industrial applications. In addition these lasers were not reliable at that time. These drawbacks were solved with development of diode-pumped solid-state high-pulse-repetition-rate lasers by “Ekspla” company. So, the need appeared to investigate opportunities of these lasers in microfabrication of material such as silicon and various metals.

Interaction of the high-repetition-rate ultrashort-pulse laser radiation with material has to be investigated. Laser radiation is focused to a very small spot, in order to obtain high accuracy of microfabrication, so the pulse energy of a few microjoules is sufficient to initiate ablation. As a processing speed is critical for practical applications, even the pulse repetition rate of several hundreds of kilohertz is often not sufficient for practical applications. On the other hand, at such a repetition rate, various side effects appear, affecting the processing speed and surface quality. These effects have to be identified so the processing speed could be estimated. At high average power a heat removal problem appears even for very short pulses. So, the maximum applicable power has to be determined.

The scientific tasks of this work

During preparation of this thesis, the high-pulse-repetition-rate lasers were developed. Suitable niches for applications of such lasers had to be found. Thus, tasks of this work were formulated carrying out on-demand and fundamental research:

- to investigate the impact of microprocessing with picosecond pulses for silicon;
- to investigate accumulation effects processing silicon and metals with high-repetition-rate lasers;
- to find out optimal focusing conditions to maximize the energetic ablation efficiency;
- to determine the experimental procedures for optimization of processing parameters;
- to investigate the opportunities of nanoparticle generation by laser ablation in a liquid medium.

Statements to be defended

1. The maximal ablation rate of a material using the fixed pulse energy can be achieved by selecting optimal focusing conditions, when laser fluence at the center of the Gaussian beam is 7.4 times higher than the ablation threshold of the material.
2. During laser cutting of silicon in the air, doping of the laser-cut surface with carbon takes place at a depth of up to 5 μm from carbon dioxide in the ambient, and the resulting silicon carbide has influence on the surface quality of the cut.
3. Heat abstraction from the workpiece, during laser cutting of stents from Nitinol, limits the applicable average laser power and the effective cutting speed.
4. Picosecond laser ablation of silver and gold in the liquid generated a stable colloidal nanoparticle solution with a narrow size distribution.

Author's publications, related to thesis

Publications in the international ISI WEB of Science journals:

1. G. Račiukaitis, **M. Brikas**, P. Gečys, B. Voisiat, M. Gedvilas, *Use of High Repetition Rate and High Power Lasers in Microfabrication: How to Keep the Efficiency High?*, Journal of Laser Micro/Nanoengineering, **4**(3), 186-191 (2009).
2. **M. Brikas**, S. Barcikowski, B. Chichkov, G. Račiukaitis, *Production of nanoparticles with high repetition rate picosecond laser*, Journal of Laser Micro/Nanoengineering, **2** (3), 230-233 (2007).
3. S. Barcikowski, A. Menendez-Manjon, B. Chichkov, **M. Brikas**, G. Račiukaitis, *Generation of nanoparticle colloids by picosecond and femtosecond laser ablation in liquid flow*, Applied Physical Letters, **91**, 083113 (2007).
4. G. Račiukaitis, **M. Brikas**, V. Kazlauskienė, J. Miškinis, *Doping of silicon with carbon during laser ablation process*, Applied Physics A. Materials Science & Processing, **85**, 4, 445-450 (2006).
5. V. Lendraitis, **M. Brikas**, V. Snitka, V. Mizarienė, G. Raciukaitis, *Fabrication of Actuator for nanopositioning using Laser micro-machining*, Microelectronic Engineering (Elsevier), **83**, 1212-1215 (2006).

Publications in the international ISI WEB of Science Proceedings journals:

6. G. Raciukaitis, **M. Brikas**, P. Gecys, M. Gedvilas, *Accumulation effects in laser ablation of metals with high-repetition rate lasers*, Proc. SPIE, **7005**, 70052L (2008).
7. G Račiukaitis, **M Brikas**, V Kazlauskienė, J Miškinis, *Doping of silicon by carbon during laser ablation process*, Journal of Physics: Conference Series, **59**, 150-154 (2007).
8. *G.Račiukaitis, M.Brikas, Micro-machining of silicon and glass materials with picosecond lasers*, Proc. SPIE, **5662**, 717-721 (2004).

Publications in other scientific journals:

9. M. Grishin, S. Jacinavičius, G. Andriukaitis, **M. Brikas**, G. Račiukaitis, *High power and repetition-rate lasers for microfabrication*, Acta Universitatis Lappeenrantaensis, **273**, 227-238 (2007) ISBN 978-952-214-412-6, ISSN 1456-4491.
10. **M. Brikas**, G. Račiukaitis, M. Gedvilas, *Accumulation effects during processing of metals and silicon with high repetition-rate lasers*, Acta Universitatis Lappeenrantaensis, **273**, 645-656 (2007) ISBN 978-952-214-412-6, ISSN 1456-4491.

Summary of doctoral thesis

Introduction

In this part of the dissertation, the relevance of the investigation is motivated and the main task and propositions to defend are formulated.

Chapter I. Laser radiation properties and interaction with material

In this chapter laser beam properties and interaction with material are discussed. Radiation absorption and laser ablation were discussed on the basis of a two temperature model. Three different regimes were distinguished for femtosecond, nanosecond and picosecond pulses. Reasons and consequences of thermal effects were evaluated. Plasma formation and interaction with laser pulse were estimated. Material during laser ablation is removed in the form of nano-scaled particles, so mechanisms of formation and production of colloid solutions are described.

Chapter II. Review of laser microfabrication studies

In this chapter previously performed experiments were described. Works on ablation threshold and accumulation effects for various metals and silicon were discussed. A lot of attention was paid to compare ablation speeds, quality and possible applications of silicon and metal microfabrication using various radiation sources. Nanoparticle generation from metal targets and possibility of their applications were discussed.

Chapter III Methods of laser micromachining analysis

In this chapter laser microfabrication systems and sample analysis methods are described.

Lasers used in micromachining experiments are given in Table. 1.

Table 1 Laser sources used for laser processing investigations.

Model	Manufacturer	Pulse length	Wavelength, nm	Pulse energy, mJ	Repetition rate, kHz
PL2241	Ekspla	60 ps	1064	3	0,25
NL640	Ekspla	10 ns	1064	0.15 – 0.6	40
PL10100	Ekspla	10 ps	1064	0.1 – 0.2	100
Rapid	Lumera	15 ps	1064	0.001 – 0.1	600
Staccato	Lumera	10 ps	1064	0.2	50
Superspitfire	Spectra Physics	130 fs	800	1	1

Two beam guiding and sample positioning systems were used in experiments. Experimental set-up using a galvanoscanner is given in **Fig. 1 (a)**. Scanlab's ScanGine 14 galvanoscanner was used equipped with 160 mm flat field or 100 mm tele-centric lenses.

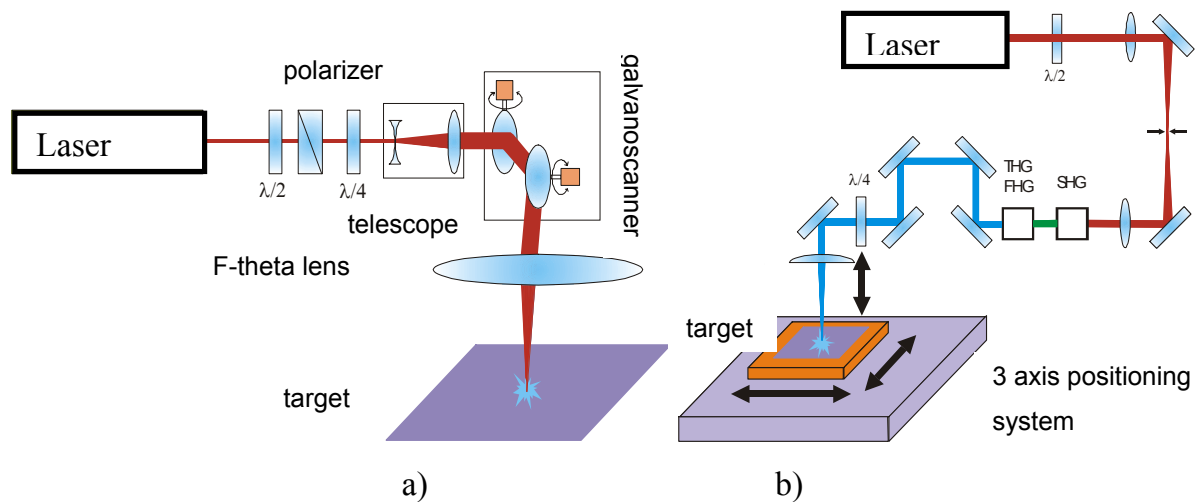


Fig. 1 Experimental set-up: a) using a galvanometer scanner; b) using a three axis positioning system.

Experimental set-up with the 3 axis precision positioning system is given in **Fig. 1 (b)**. Large variety of optical elements for laser beam transformation and various focusing lenses were used in this set-up.

Fundamentals of surface analysis methods – x-ray photoelectron spectroscopy, secondary ion mass spectroscopy and Auger electron spectroscopy – are given in this chapter.

Chapter IV Ablation with high repetition rate nanosecond and picosecond pulses

Ablation threshold and accumulation effects

Intensive laser radiation affects properties of the material surface in such a way that the material becomes more sensitive to laser radiation and the energy density required for material removal decreases several times. The dependence of the ablation threshold on the pulse repetition rate and the number of pulses applied to the test material was investigated. All tests were performed with picosecond and nanosecond pulses and the effect of shorter pulses is discussed. Experiments were performed on stainless steel, copper, aluminium and silicon.

Craters were formed in the surface when laser fluence was above the ablation threshold. Separate craters were ablated with 1, 10, 100 and 1000 laser pulses at a given laser pulse energy, and experiments were repeated using a set of laser pulse energies. For evaluation of the ablation threshold we used the method introduced by J.M. Liu [7] valid when the Gaussian beams are applied. The diameters of craters were measured with the optical microscope and plotted versus laser pulse energy used to ablate the crater. The threshold was estimated from the relationship between the laser fluence F_0 and the diameter D of a crater etched with a pulse:

$$D^2 = 2\omega_0^2 \ln\left(\frac{\phi_0}{\phi_{th}}\right), \quad (1)$$

where ω_0 denotes the beam waist and F_{th} is the threshold fluence. Linear fitting of the data was performed in representation of experimental data as $D^2 = f(\ln(E_p))$. The waist radius was estimated at the first step from a slope of the fitting line, and the value of the laser pulse energy E_p was converted to the laser fluence.

The ablation threshold for stainless steel, copper, silicon and aluminium irradiated with the picosecond laser was estimated from the crater diameters using the J.M. Liu method [7] and results are given in **Table 2**.

Table 2. Ablation thresholds for 10 ps and 6 ns laser pulses.

No.	Pulse length	Wavelength	Material	Ablation threshold, J/cm ²			
				1	10	100	1000
1	10ps (PL10100)	1064 nm	Stainless steel	0,5	0,2	0,1	0,04
2			Aluminium	0,85	0,47	0,16	0,15
3			Copper	1,73	0,74	0,5	0,33
4		532 nm	Silicon	0,44			
5	10 ps (Lumera Rapid)	1064 nm	Silicon			0.59	0.45
	6ns (NL640)	1064 nm	Stainless steel	7,3	4,6	4,2	3,3
6			Aluminium	3,2	2,3	1,8	1,6
7			Copper	8,8	6,6	6,8	6,7
8	60ps (PL2241)	266 nm	Silicon	0.17			

The incident laser power (pulse energy) was used instead of the absorbed one in evaluations as was also done in [8,9]. It is not correct regarding parameters of the material because most of the energy was reflected by the metal surface. Metals reflect about 70-99% of laser radiation in the near infrared range. It is technically difficult to measure the laser energy coupled to the workpiece but in our case the ablation threshold was sensitive to surface finishing conditions. No special attempts were made to prepare the surface of specimens before experiments, such as chemical or electro-chemical polishing [10].

According to the accumulation model of Jee et al. [10], the ablation threshold and the number of laser pulses used to ablate a crater are related by an equation:

$$\phi_{th}(N) = \phi_{th}(1)N^{S-1}, \quad (2)$$

where $0 < S \leq 1$ is the accumulation coefficient, which describes incubation of defects after laser irradiation. $S = 1$ means that no incubation appears and the ablation threshold does not depend on the number of laser pulses. A typical value for metals is $S = 0.8-0.9$. If the parameter S is larger than 1, the specimen surface is hardened by laser irradiation. The ablation threshold can be influenced by the initial state of the surface. The surface roughness and contamination increase absorption, and therefore the energy input to the material.

Ablation rate

The ablation rate was estimated in the bulk metal specimens using both lasers. Rectangular cavities with the lateral dimension of $1 \times 1 \text{ mm}^2$ were milled in the metals with multiple (8 millions) laser pulses. The depth of the holes was measured using an optical microscope, and an ablated volume was calculated. The depth of laser milled cavities varied from 35 to 300 μm . The mean ablation rate in $\mu\text{m}/\text{pulse}$ was estimated dividing the cavity volume by the pulse number and the laser spot area. As the milled area was large compared to a laser spot, the shielding effects of a confined crater [11] had no impact on the results.

The ablation rate increased with the laser pulse energy and power but deviation from linearity was remarkable. A slower rise of the ablation rate at higher pulse energies was observed.

The repetition rate was kept constant (50 kHz), while the pulse energy and the average power were controlled simultaneously by an attenuator. Saturation in the rise of the total ablation rate was approved at a higher laser power. The ablation efficiency was limited by phenomena that were excited at the high intensity of laser radiation. The results were transformed into the energetic ablation efficiency in $\mu\text{m}^3/\text{mJ}$, the volume of the material ablated with a portion of energy. Both parameters are mean values of impact of more than a million laser pulses and represent the real efficiency of laser processing. Fig. 4 shows the energetic ablation efficiency in $\mu\text{m}^3/\text{mJ}$ as a function of the mean laser power. Since every milijoule of the NL640 laser energy was able to remove more material at a higher average power of the laser (higher repetition rate), a significant fall in the energetic efficiency was found using the picosecond laser at a higher power. The intensity of absorbed laser radiation was estimated for both lasers and it was compared to the intensity of plasma ignition of metals ($2 \times 10^{13} \text{ W}/\text{m}^2$). Fig. 2 shows experimental data of the energetic ablation efficiency of steel, nickel and aluminium with the picosecond laser.

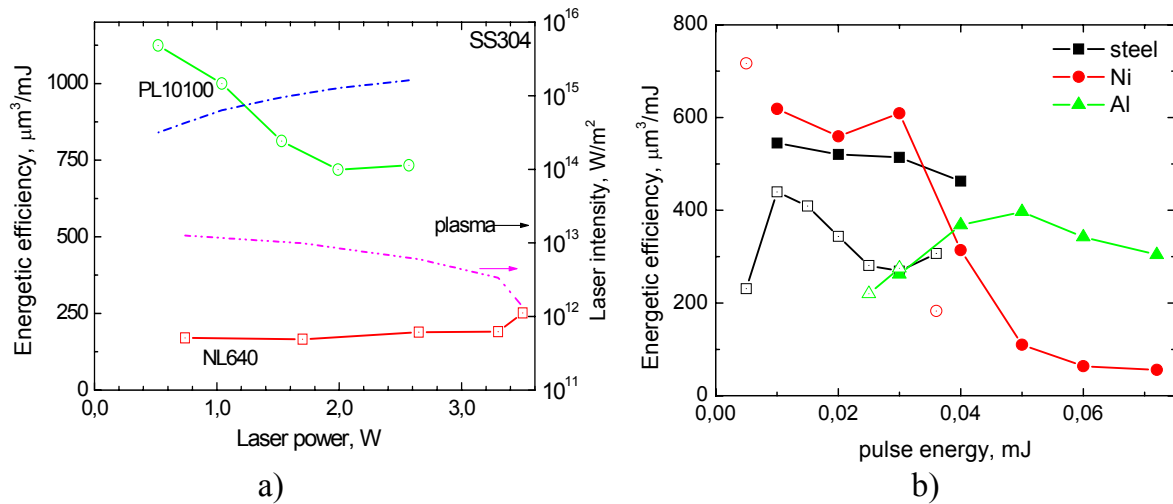


Fig. 2. Energetic efficiency of laser ablation of stainless steel with the picosecond and nanosecond lasers. Dotted lines show intensity of laser radiation absorbed in the specimen. The plasma formation threshold is indicated. Ablation efficiency in metals with the picosecond laser at the 50 kHz (filled dots) and 100 kHz (open dots) repetition rate.

The data were evaluated at two different pulse repetition rates and are plotted versus the pulse energy. A significant fall in the energetic efficiency occurred using the picosecond laser at a higher power. The evaporation efficiency in $\mu\text{m}^3/\text{mJ}$ was higher for the pulse repetition rate of 50 kHz (filled dots) compared to 100 kHz (open dots) at the same pulse energy in case of all examined metals, except aluminium. The repetition rate had no effect on the energetic ablation efficiency in aluminium. Nickel showed a large drop in the efficiency in a narrow range of pulse energies.

Specific pulse energy, which gives the maximal ablation efficiency exists under certain focusing conditions. Reflectivity of aluminium is 91% and reflectivity of nickel is 70% for 1064 nm radiation. Thus, the input energy for aluminium sample should be three times higher to get the same absorbed energy. This explains why the ablation efficiency curve for aluminium is shifted to higher energies.

Optimization of laser beam focusing

Modelling and experiments were performed to establish relations between the laser ablation efficiency in terms of the material removal rate with parameters of the laser beam: the spot size, pulse energy or fluence. Modelling was based on the idea of Furmanski et al. [12]. The model is a simplified view of the laser ablation. It does not

take into account any reflection from the surface, including tilted crater walls. The whole laser energy is coupled in a narrow layer of the material according to the Beer law. Any energy losses due to heat conduction and plasma absorption are excluded. The assumption is valid quite well in case of ultra-short pulses when the heat diffusion during pulse duration is less than the absorption depth. The analysis was performed in order to determine relations between the laser and material parameters as well as the efficiency and precision of laser fabrication by ablation.

Laser microfabrication is based on the use of multiple laser pulses to ablate the material. When a burst of laser pulses is applied together with scanning, every new pulse hits the workpiece surface Δx or by a beam overlap in % as follows $(2w_0 - \Delta x)/2w_0$. The profile of the trench made by partially overlapping laser pulses can be calculated. So, the evaporation rate (volume per time) can be estimated when the pulse repetition rate R_{rep} and the shift between pulses are taken into account:

$$\frac{dV}{dt} = R_{rep} S \Delta x = R_{rep} \frac{\delta \pi}{6} \ln \frac{F_0}{F_{th}} \left(\frac{3w_0^2}{2} \ln \frac{F_0}{F_{th}} - \Delta x^2 \right). \quad (3)$$

The relationship between the evaporation rate and the laser pulse energy as well as the fluence is non-linear. By varying focusing of the beam is it possible to reach maximum in the evaporation rate of the material.

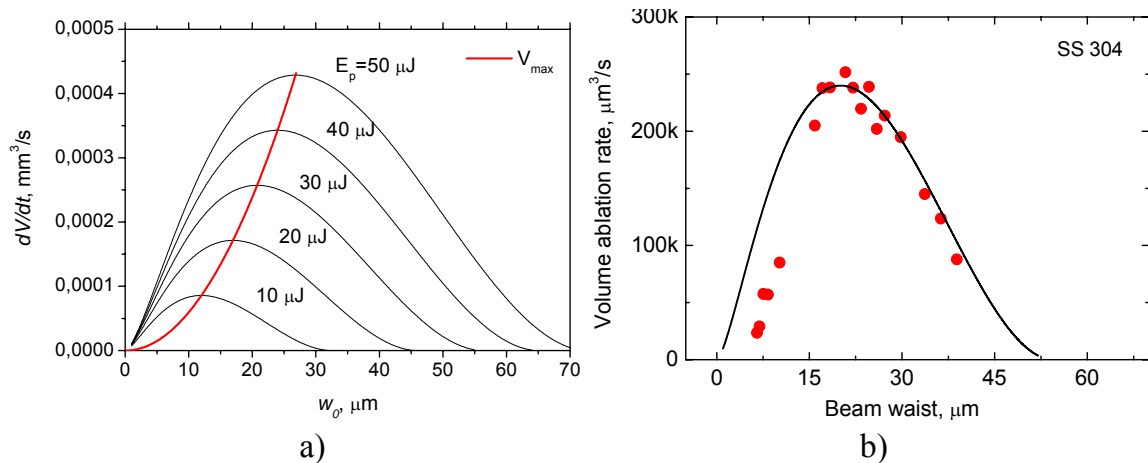


Fig. 3 Material re-removal rate at ablation of the trench by a burst of laser pulses depending on the laser beam waist at fixed pulse energies. $F_{th}=0.6 \text{ J/cm}^2$, $\delta=0.038 \text{ } \mu\text{m}$, $R_{rep}=50 \text{ kHz}$, $dx=0.1 \text{ } \mu\text{m}$. a) modelling; b) measured values at laser pulse energy of $28 \text{ } \mu\text{J}$.

For every given set of laser pulse energy E_p , the ablation threshold F_{th} and the distance between subsequent laser pulses Δx , it is possible to define the beam waist when the evaporation rate is maximal (**Fig. 3a**). If the shift between subsequent laser pulses is much less than the beam radius, the optimal beam waist is the same as in case of the single pulse ablation. The most efficient material removal takes place when the laser fluence is equal to:

$$F_{0 \max} = e^2 F_{th} \approx 7.4 F_{th}. \quad (4)$$

The expression for the maximal evaporation rate at the optimal laser beam focusing can be written:

$$\left(\frac{dV}{dt} \right)_{\max} = R_{\text{rep}} \frac{2\delta E_p}{e^2 F_{th}} \left(1 - \frac{\Delta x^2}{w_{0 \max}^2} \right) \approx R_{\text{rep}} \frac{2\delta E_p}{e^2 F_{th}}. \quad (5)$$

The evaporation rate depends on material properties (absorption depth and ablation threshold) and parameters of the laser beam (pulse energy, repetition rate). The pulse energy and the repetition rate linearly affect the evaporation rate. Therefore, these laser parameters are topmost important for scaling the efficiency of laser microfabrication.

Experimental verification of the modelling results was performed by ablating trenches in stainless steel at variable focusing. The depth profiles of the trenches were measured with a stylus profiler. At a given scanning speed, the evaporation rate dV/dt was calculated and it is shown as a function of the beam waist at the constant pulse energy (**Fig. 3b**).

Good correlation between calculated and experimental data was found when the beam waist was large enough or the laser fluence was not too high. Deviations of the experimental data from estimations occurred in an opposite case and could be related to the limitation of the stylus profiler to measure deep and narrow trenches which were formed at tight focusing and high laser fluence. The geometrical limitation of the stylus led to the underestimated value of the trench cross-section.

Chapter V Microprocessing of silicon with picosecond lasers

Single-shot patterning of silicon was performed at a few laser pulse energy settings and at a few focal positions above and behind the surface. A single-shot crater made at 12 J/cm^2 was analysed in details. When the beam diameter above the ablation threshold was $27 \text{ }\mu\text{m}$, the resulting crater depth was $0.8 \text{ }\mu\text{m}$. Recast material was spread within the diameter of $42 \text{ }\mu\text{m}$ with the burr height of $0.3 \text{ }\mu\text{m}$. Taking into account cylindrical symmetry of the crater, the total volume of recast material was about 70% of that of the crater. As density in the recast area is lower than in the bulk material, about 30-50% of the ablated silicon was left in close surroundings of the crater after the very first pulse. The recast was formed mainly by melt expulsion during vapour expansion from the ablation zone. A significant impact of the melt phase in ablation process of silicon was established at 60 ps pulse duration. According to the investigations made by Luft et. al. [13] in silicon at high laser fluences, a recast layer on walls does not disappear even for 200 fs pulses. Heat from the recast material stimulates the formation of a heat-affected zone (HAZ) irrespective of the applied pulse duration. In case of picosecond laser ablation of silicon HAZ reaches less than $5 \text{ }\mu\text{m}$. The results for silicon are in agreement with the results obtained in metals [14,15].

The laser processing experiments on silicon wafers p-Si {111} with the thickness of $550 \text{ }\mu\text{m}$ were carried out with the lasers of various pulse durations: 60 ps and 130 fs. The range for “gentle” ablation of silicon with a picosecond laser had been defined in [16] and all the experiments were performed below the limit of crack formation. Cutting was performed by multi-pass scanning along the cutting line. The pulse energy and spot overlap as well as the number of passes were varied during the experiments. For experiments in the controlled atmosphere, the samples were incorporated inside the vacuum chamber with a window of fused silica. Vacuum was created with a rotary pump and the chamber was later filled with nitrogen. In order to define the thickness of the

layer disturbed by laser cutting of silicon, a set of samples was prepared with the lasers using various pulse durations, wavelengths and settings of laser power.

The cutting experiments of silicon wafers were performed by multiple scans along the cutting line. The UV radiation of 266 nm assisted faster penetration through the wafer compared to IR radiation of the nano- and femtosecond lasers at the same fluence. On the other hand, the volumetric ablation rate for the femtosecond laser with similar fluence was higher, leading to the higher cutting speed. The original laser-cut surface had a prismatic-edged structure (“channels”) on it orientated in parallel with a laser beam.

The layer affected by laser cutting was analyzed by various techniques. AES, XPS and SIMS investigations were performed with the surface analysis equipment. Roughness of the surface and conglomerates formed by photo-chemical reactions during laser cutting could distort the results. They caused the different local etching rate or efficiency of photoemission. Therefore, it was difficult to match the etching time with the depth. Characterization of the chemical composition and the chemical bonding of the laser cut edge were performed by XPS. A focused beam of Ar-ions was used in secondary ion mass-spectroscopy experiments, cleaning of surfaces after incorporation into the vacuum chamber and etching the depth profiles. Auger-electrons were excited with the electron beam with a spatial resolution of 2.5 μm . The elemental profile was measured on the surface freshly cleaved in the air and cleaned with Ar-ions in vacuum.

X-ray electron spectroscopy

X-ray photoelectron spectroscopy was used to characterize the surface layer. The peaks from Si $2p$, C $1s$, N $1s$ and O $1s$ were observed in the XPS spectra. These peaks showed that the surface layer consisted of Si, N, C and O elements. Investigation of a fine structure of the XPS spectra enabled resolving spectral components, the relative intensity of which was dependent on the sample preparation. The main component of the Si $2p$ line located at 103.2 eV (Fig. 4) was in agreement with the position of the SiO₂ peak in thermally oxidized silicon. The position of the low energy peak (98 eV) was in agreement with the neutral state of a silicon atom [17]. Additional components

corresponding to intermediate ionization states of silicon were found between the latter in spectra of all samples cut with the laser in the air independently of the pulse duration and wavelength. They were related to Si–C bond (100.45 eV) and pseudo-morphous configurations of silicon oxo-carbide Si–O–C (102.1 eV) [18]. As the formed layer of oxide was thinner when the low-power laser was used for cutting, the Si⁰ line emerged after prolonged etching (10 min). UV radiation of 266 nm was able to create a thick oxide layer at considerably lower power, and it was impossible to remove the oxide during the 10-min etching. The relative intensity of the SiC component increased after etching. This is an indication that small carbon atoms penetrated deep into the sample, while the surface was glutted with oxygen. Residual gases in the chamber and bad heat dissipation at reduced pressure led to creation of an oxide film during laser ablation in the rough vacuum. Si–N bonds were detected in the sample cut in nitrogen.

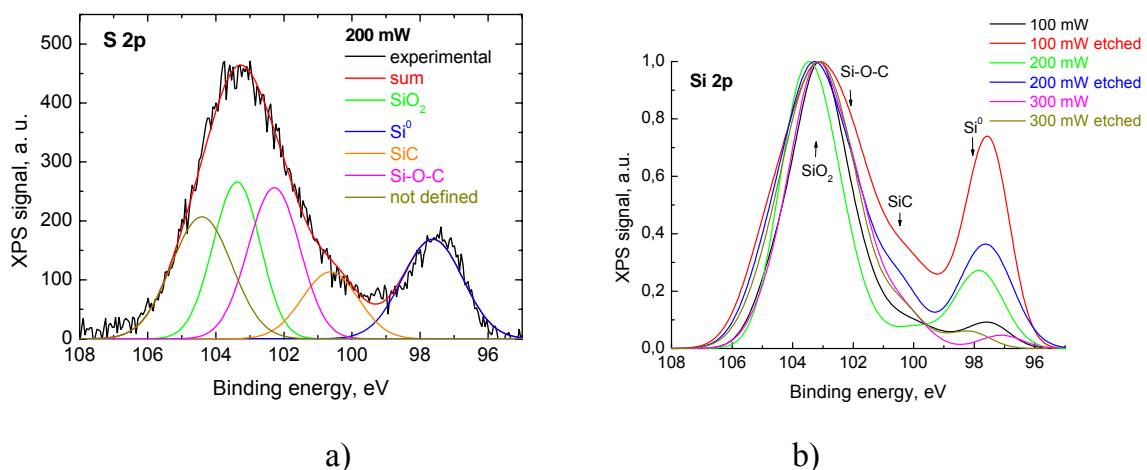


Fig. 4. Normalized XPS spectral Si2p line: a) as cut; b) after etching with Ar⁺ ions.

Their position at about 102 eV in the Si 2p line overlapped a peak of the Si–C bonds, but SiC ions were not observed by SIMS in the sample cut in nitrogen. The peak of elemental silicon (Si⁰) was clearly detected in the sample cut in nitrogen. The carbon C1s line of laser cut samples remained in the XPS spectra after ion-beam etching, while adsorbed hydrocarbon shortly disappeared from the surface of the thermally oxidized silicon. The same was found in the behaviour of the C1s line of the sample cut in the air, when the central part responsible for the –CH bond, disappeared after etching (Fig. 5).

The line transformed into the twin-peaked one with the low energy peak located at 282.4 eV (C–Si bond). The other C1s peak at about 286.3 eV is a typical characteristic of oxidized carbon species, in particular carbonyl species of the CO type [19], or could also be associated with the Si–O–C bond [20].

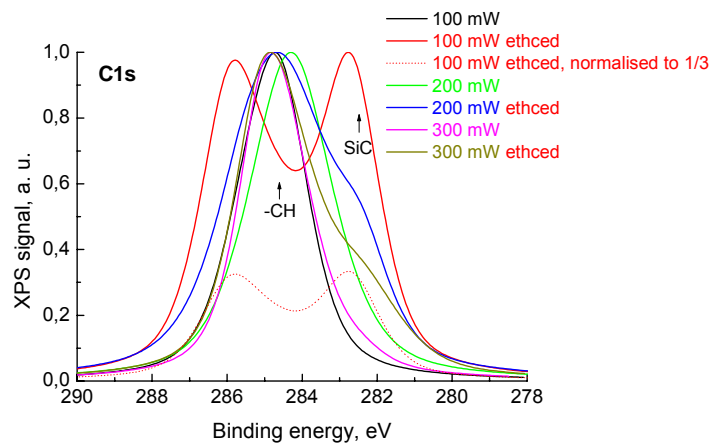


Fig. 5. Normalized XPS spectra of the C1s line.

Secondary ion mass-spectroscopy

SIMS spectra of all the samples were measured twice: without special treatment and after ion-beam etching for 5–10 min. Different combinations of Si, O, C, and in some samples N ions were detected. In the SIMS spectra of the laser-cut surface of silicon, the most distinguished were the triple lines of Si^+ (28, 29, 30) and SiC^+ (40, 41, 42), relative intensity of which corresponded to natural abundance of Si^{28} , Si^{29} and Si^{30} isotopes. The preventing effect of the shielding atmosphere of nitrogen and vacuum against carbon incorporation was confirmed by SIMS measurements as radical changes appeared in the range of ion mass 40–42 (SiC). Conglomerates of ions originated from silicon and silicon with oxygen or carbon atoms were identified in the SIMS spectra, while different groups of ions combining silicon with nitrogen were detected in the wafer heated in vacuum at the temperature above 900°C and exposed to the atmospheric air. No conglomerates were found in SIMS spectra of the cleaved surface.

The depth profile was measured during prolonged etching with the Ar^+ ion beam. The etching rate was fourfold slower in the area of the “channel” formation compared to the upper part of the edge. Relative intensity of the lines changed during the process and

reflected spatial distribution of different species. Even at cutting with the femtosecond laser the disordered layer was found to be of the 2 μm thickness (Fig. 4). Elemental carbon disappeared faster than its combination with silicon. The SiC formations were incorporated below the surface. Behaviour of silicon sub-oxides was stipulated by the depth profile of oxygen.

Auger electron spectra

The sample cut in the air with the 266 nm radiation was prepared for AES measurements by fresh cleavage of the wafer perpendicular to the laser cutting line. The cleaved surface was cleaned by Ar-ions after placement in vacuum. Scans with the electron beam (3 keV) were performed on the cleaved surface in parallel with and perpendicular to the laser-cut surface. Start points of the scans were 3–5 μm off the corresponding rim. The peak-to-peak height of each element and the atomic sensitivity factor were used for quantitative analysis. Two different positions were used for scanning out of the region of “channel” formation, and an identical shape of the concentration profiles was found. Both positions (depth) are marked in Fig. 6 by X1 and X2. The accuracy of concentration estimation was 10%. Residual contamination of adsorbed hydrocarbons caused the observed background concentration of carbon far away from the surface processed by the laser (X-direction).

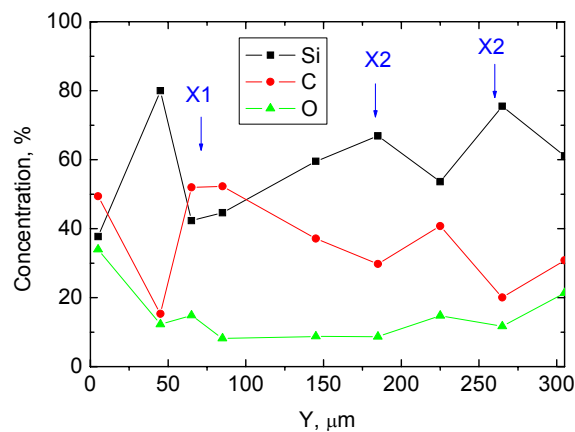


Fig. 6. Distribution of Si, C and O atoms in the silicon wafer close to the laser cut surface along the cutting depth (in parallel). Positions of scans in perpendicular directions are shown (X1, X2). Two different positions were used for scanning out of the region of “channel” formation and, a similar shape of the concentration profiles was found at the positions X2.

Concentration profiles measured in parallel with the laser-cut wall at the 15–18 μm distance from it showed non-uniform distribution of impurities. High concentration of oxygen and carbon was detected close to the laser-entry surface. This part of the cut was most influenced by the native surface of the wafer. Both sides of the wafer were not polished after sawing from the bole. The upper part of the cut also had the longest contact with the UV laser beam and plasma created during ablation. Carbonization of the layer was minimal at the depth of 50 μm , while concentration of oxygen fell down at this depth.

In the area where the channels were formed during laser cutting, high concentration of carbon was detected again. The deeper penetration of carbon at this depth was determined by a perpendicular scan.

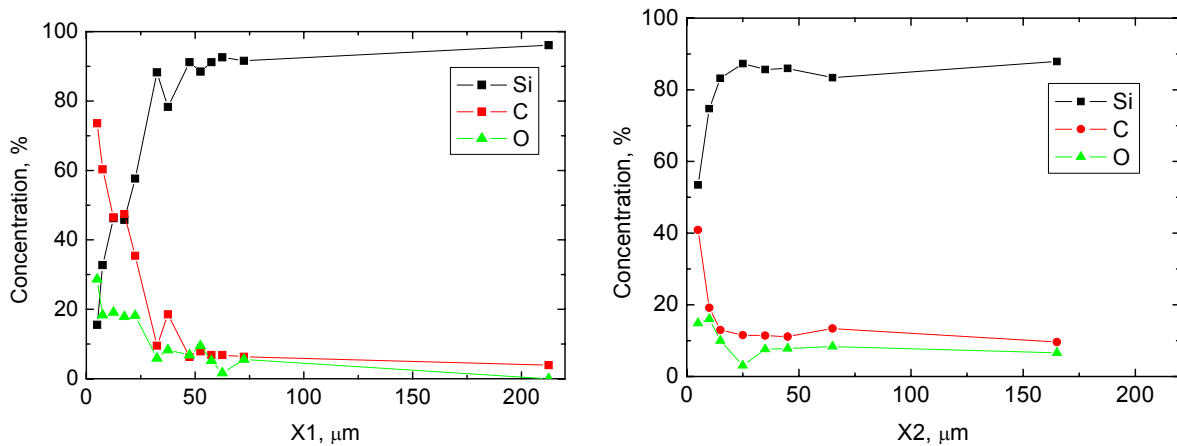


Fig. 7. Distribution of Si, C and O atoms in the silicon wafer close to the laser cut surface, perpendicular to it: filled points– at the depth of channel formation (X1); open points – at laser depth (X2).

The carbon concentration profiles measured by AES in the sample #4 cut with the 1064 nm radiation are shown in **Fig. 7**. Scanning was performed in parallel with the laser cut wall. The central part of the sample near the laser cut surface was again enriched with carbon ions. The penetration depth of carbon was estimated to be up to 25 μm from the laser-cut surface into the bulk of the material. Because of the surface roughness, there was no strict reference point for the depth measurement. The laser-cut wall was like a sandwich, formed from the heat-affected zone in the bulk, the layer of melt with

possible voids and deposits on the top. Assuming the starting point to be the middle of the kerf (40 μm on the entry side), at least a 5 μm layer of bulk silicon was doped with carbon during laser cutting.

Chapter VI Applications of high-repetition-rate picosecond lasers in microfabrication

Surface roughness and ablation regimes

Metal ablation tests were concentrated on the formation of 3D structures. New requirement for surface roughness and precision of geometry appear (**Fig. 8**). Surface roughness test was performed using the Lumera Rapid laser. The laser pulse length is 10 ps, scanning speed - 200 mm/s, hatch - 0,002 mm every structure was scanned 5 times. The laser was operating at full output power, which is rated at this pulse repetition rate. Therefore, both the total power and pulse energy were changed. It is clear that surface roughness in these samples differs radically. As the change of the pulse repetition rate changes the pulse overlap, it is logical to think that it is possible to find out an optimal set of parameters for the lowest surface roughness.

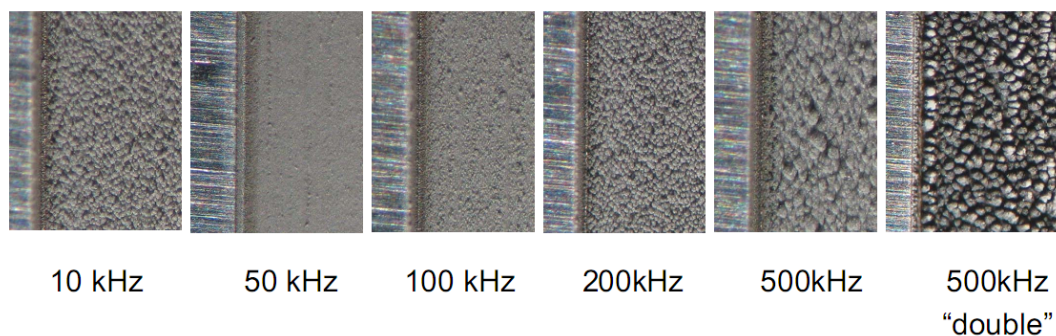


Fig. 8 Dependence of surface quality on ablation parameters for aluminium.

For investigation of surface roughness a set of experiments was made. Hatch, the number of scans and pulse energy were varied. Nickel and copper samples have been chosen. Besides two different laser sources (Ekspla PL10100 and Lumera Staccato) were

used. Different laser sources give different intensity profiles at focus, so roughness parameters differ for a certain set of parameters.

Formation of 3D structures in metals

Instrumental steel ablation experiments were carried out using picosecond pulses. Scribing and 3D structure forming were tested. Laser radiation of 1064 nm and 355 nm was focused to the beam waist of 30 μm . Samples of 3D structures in instrumental steel are shown in **Fig. 9**: stepped structure (a) and hemisphere (b).

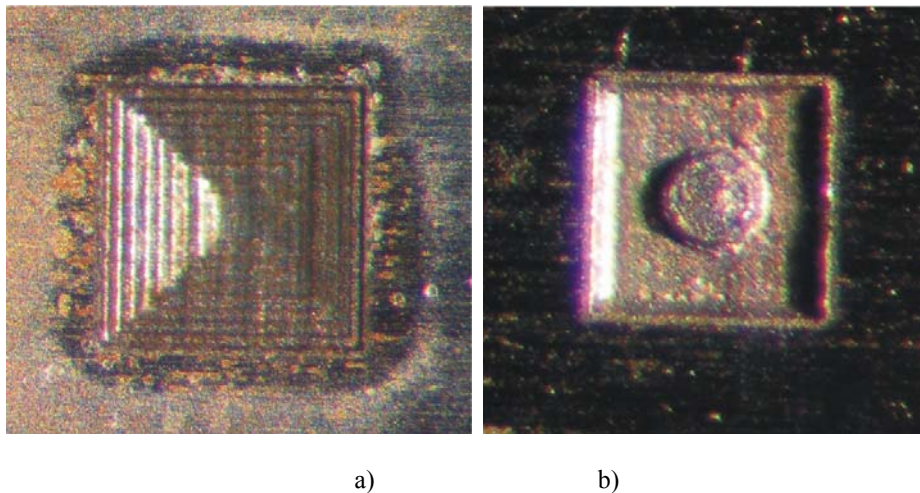


Fig. 9. 3D structures in instrumental steel: stepped pyramid structure (a) and hemisphere (b).

Laser processing of Nitinol

Nitinol, the nickel and titan alloy, has unique characteristics such as superelasticity and shape memory. This chemically neutral alloy is widely used in medical applications. Mechanical processing methods are not suitable for fabrication of micromanipulators or stents, and short pulse lasers here have an opportunity due to very low thermal effects. Average surface roughness of 0.2 μm can be achieved by femtosecond laser ablation, thereby the thickness of the debris layer is lower than 7 μm and the hardened layer is thinner than 70 μm [21]. The laser pulse length was 150 fs and energy 0.8 mJ. Nitrogen gas was used to prevent surface oxidation. Reduction of the pulse energy leads to lower thermal effects and better surface quality.

Stent cutting using high repetition rate picosecond lasers

Experiments at “Laser Zentrum Hannover” research center were held using the picosecond laser PL10100, for cutting stents from Nitinol tubes. It was expected, that usage of the high pulse repetition rate laser for small diameter stent cutting can lead to a higher processing speed and better accuracy.

Performing cutting tests, the optimal cutting speed of 2 mm/s (two scans at 4 mm/s) has been reached. The highest applicable power of 4 W was limited by heat dissipation. The cut width was 9 μm .

Stent cutting was performed at selected regimes. Due to complex configuration and narrow cut width it is very hard to remove the cut parts. On the other hand, a very fine stent structure is not able to sustain the 4 W average power, so, it had to be reduced to 3 W (Fig. 10). This led to a slower processing speed.

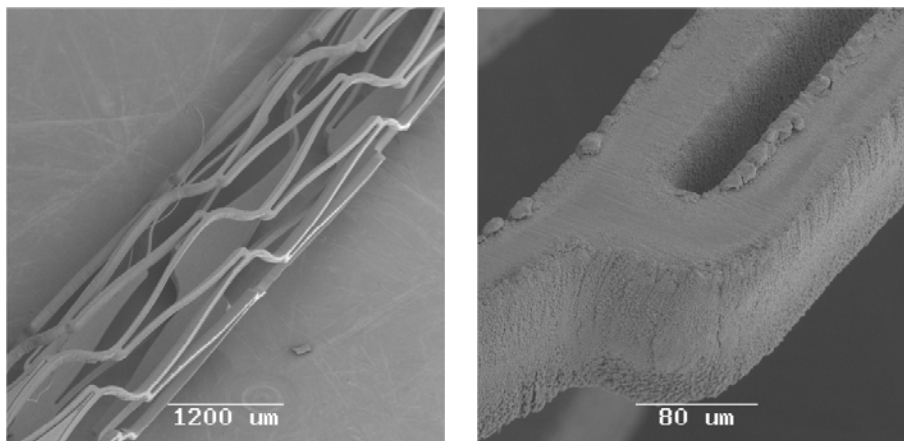


Fig. 10 Stent cut at 3W average power, 100 kHz pulse repetition rate and 0.2 mm/s effective speed.

It is very difficult to define the exact number of scans for a stent because parts are very hard to remove due to a narrow cut width. A higher number of scans increases the cut width and polishes the wall. This makes the part removal easier.

Sample shown in Fig. 10 meets all requirements to surface roughness, flexibility and strength, however, the processing speed of 0.2 mm/s is too slow for commercial applications.

Chapter VII Generation of nanoparticle colloids by picosecond laser ablation in liquid flow

The fabrication of silver and gold nanoparticle colloids using the picosecond (10 ps) laser ablation in liquids was studied. A commercially available picosecond laser (Ekspla PL10100) working at 5.5 W and 1064 nm laser wavelength and the pulse repetition rate up to 100 kHz was used for the fabrication of metal colloids in liquids. A 50 mm lens focused the laser beam.

A special cell for nanoparticle production was constructed for this experiment (**Fig. 11**). Liquid in the cell was mixed with the magnetic stirrer. This led to minimization of the influence of thermal-lens effects and faster bubble removal from the process zone.

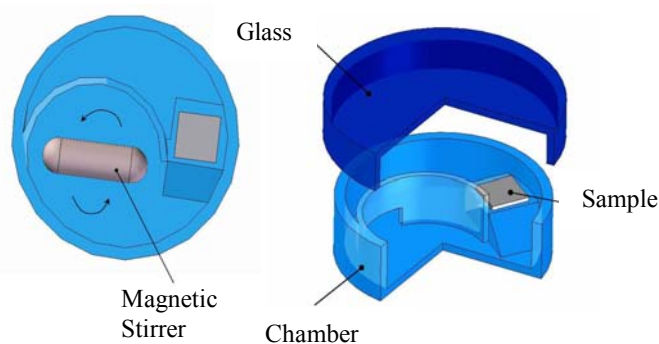


Fig. 11 Design of the stirred cell for nanoparticle production.

The maximum nanoparticle productivity obtained for 10 ps laser pulses was 8.6 $\mu\text{g/s}$ at the 50 kHz repetition rate (110 μJ) and 6.8 $\mu\text{g/s}$ at the 100 kHz repetition rate (60 μJ). The difference appeared due to higher ablation efficiency at the higher laser pulse energy. The produced nanoparticles were analyzed with the scanning electron microscope (SEM) (**Fig. 12 a**).

The spatial resolution of SEM was about 20 nm, therefore there is no information about smaller nanoparticles. The most probable diameter was 50 nm and the size of nanoparticles varied from 30 to 80 nm (**Fig. 12 b**).

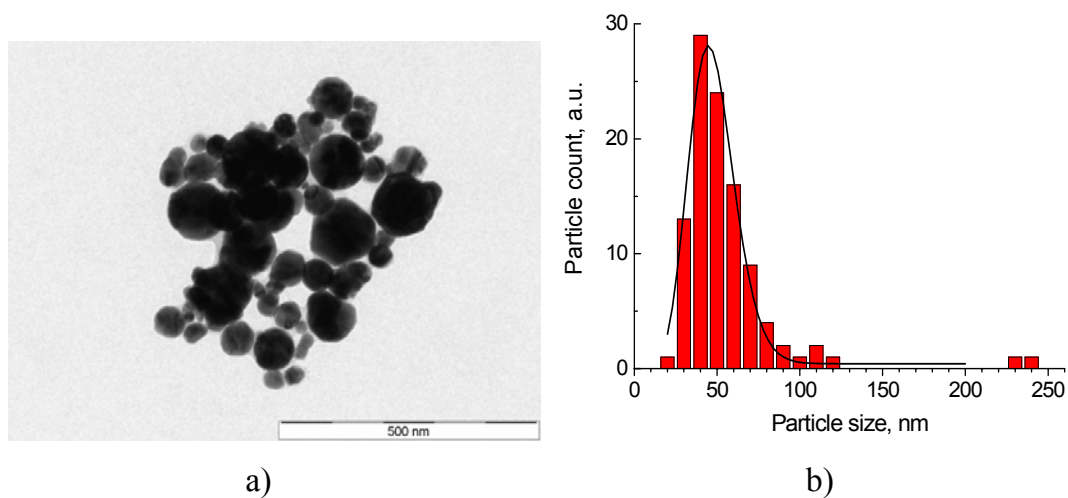


Fig. 12 a)TEM picture of silver nanoparticles made at 100 kHz, 5.5W, b) Size distribution of silver nanoparticles produced by the picosecond laser ablation in water.

The same laser equipment was used to produce gold nanoparticles in n-hexane. A stabilizing agent was used to prevent agglomeration because the hexane molecules have no dipole moment. Concentration of the stabilizing agent dodecylthiol was changed in order to check stabilization properties. It was varied from 8 to 2 mmol/l. The processing time was 240 s and the mass removal varied at about 0.9 mg (ablation rate 5.9 $\mu\text{g/s}$) at the 5.5 W output power and the 50 kHz pulse repetition rate.

Conclusions

1. The ablation threshold decreases when several pulses are applied due to incubation of defects. Accumulation effects are stronger for picosecond than nanosecond pulses and this can be caused by stronger shockwaves for shorter pulses.
2. The volumetric ablation efficiency non-linearly depends on the laser pulse energy. The model which allows determination of optimal beam focusing conditions for maximum evaporation rate at given pulse energies, was developed. The maximal ablation rate of the material was achieved when laser fluence in the center of the Gaussian beam was 7.4 times higher than the ablation threshold of the material.

3. Optimal focusing conditions limit the precision of machining due to a large spot size in focus. Therefore, the process parameters have to be intelligently controlled for fast machining and effective energy usage, combining rough and fast machining with accurate and slow one.
4. It has experimentally been defined that the energetic ablation efficiency at high pulse energies is limited due to plasma shielding. The increase of laser pulse energy is not an effective way to increase productivity. The laser beam split and parallel processing can be applied for efficient application of high pulse energy lasers in microfabrication.
5. Empirical relationships were found between process parameters and machining performance of silicon for laser percussion drilling and cutting.
6. The contact of silicon with air molecules during the ablation process in the presence of laser radiation and laser-ignited plasma initiated thermo-chemical reactions. The thermal gradient stipulated diffusion of surface-adsorbed ions, leading to doping of silicon with carbon. Silicon carbide type bonds were formed below the surface and could be the reason for “channeling” at the wafer cut. Shielding gas of nitrogen can prevent carbonization of the surface.
7. Picosecond lasers were used for cutting the electrostatic micro-positioning actuator from silicon and forming 3D structures in instrumental steel and nitinol.
8. Laser-machined surface quality depends on process parameters and the minimum value of $R_a = 130$ nm is achieved for a copper sample.
9. Heat abstraction from the workpiece, during laser cutting of stents from nitinol, limits the potential use of the average laser power and the effective cutting speed.
10. The picosecond laser can effectively generate nanoparticles of a narrow size distribution in liquids. The silver nanoparticle generation rate in water was $8.6 \mu\text{g/s}$ at 5.5 W average laser power and 50 kHz repetition rate. Gold nanoparticles were generated at $5.9 \mu\text{g/s}$ rate in n-hexan medium. Nanoparticles produced by laser ablation are stable for a long time.

References

- [1] J. Perriere, E. Millon, E. Fogarassy: **Recent advances in laser processing of materials**, Elsevier Ltd. (2006), ISBN-13: 978-0-08044-727-8, ISBN-10: 0-080-44727-9.
- [2] P. M. Sarro: **M³: the Third Dimension of Silicon**, in Enabling Technologies for MEMS and Nanodevices, WILEY (2004), ISBN: 978-3-527-30746-3, pp. 1-20.
- [3] T. Tsuji, T. Hamagami, T. Kawamura, J. Yamaki and M. Tsuji: **Laser ablation of cobalt and cobalt oxides in liquids: influence of solvent on composition of prepared nanoparticles** Appl. Surf. Sci. 243, 214-219 (2005).
- [4] F. F. Mafunè, J. Kohno, Y. Takeda, and T. Kondow: **Formation and Size Control of Silver Nanoparticles by Laser Ablation in Aqueous Solution**, J. Phys. Chem. B **104**, 9111-9117 (2000).
- [5] S. Barcikowski, A. Hahn, A.V. Kabashin, B.N. Chichkov: **Properties of nanoparticles generated during femtosecond laser machining in air and water**, Appl. Phys. A **87**, 47-55 (2007).
- [6] J.-P. Sylvestre, A.V. Kabashin, E. Sacher and M. Munier: **Femtosecond laser ablation of gold in water: influence of the laser-produced plasma on the nanoparticle size distribution**, Appl. Phys. A **80**, 753-758 (2005).
- [7] J. M. Liu: **Simple technique for measurements of pulsed Gaussian-beam spot sizes**, Opt. Lett. **7**, 196-198 (1982).
- [8] P. Pantzar, H. Laakso, P., Penttilä R.: **Material removal rates of metals using UV and IR picosecond pulses**, Proceedings of the Fourth International WLT-conference on Laser in Manufacturing 2007, Munich, June 18-22, 2007, pp. 613-618 (2007).
- [9] E.G. Gamaly, N.R. Madsen, M. Duering, A.V. Rode, V.Z. Koley, B. Luther-Davies: **Ablation of metals with picosecond laser pulses: Evidence of long-lived nonequilibrium conditions at the surface**, Phys. Rev. B **71**, 174405 (2005)
- [10] Y. Jee, M. F. Becker, R. M. Walser: **Laser-induced damage on single-crystal metal surfaces**, J. Opt. Soc. Am. B **5** (3), 648-659 (1988).
- [11] D. Breitling, A. Ruf, F. Dausinger: **Fundamental aspects in machining of metals with short and ultrashort pulses**. Proc. of SPIE, **5339**, 49-61 (2004).
- [12] J. Furmanski, A.M. Rubenchik, M.D. Shirk, B.C. Stuart: **Deterministic processing of alumina with ultrashort laser pulses**, J. Appl. Phys., **102**, 073112 (2007).
- [13] A. Luft, U. Franz, A. Emsermann and J. Kaspar: **A study of thermal and mechanical effects on materials induced by pulsed laser drilling**, Appl. Phys. A, **63** (1996), pp. 93-101.

-
- [14] F. Dausinger: **Machining of Metals with Ultrashort Laser Pulses: Fundamental Aspects and their Consequences**, CLEO/Europe 2003, Munich, Germany, June 23-27, 2003.
- [15] M. Weikert, Ch. Foehl, F. Dausinger: **Surface structuring of metals with ultrashort laser pulses**, Proceedings of Third International Symposium on Laser Precision Microfabrication, Proc. SPIE **4830**, 501-505 (2003).
- [16] G. Račiukaitis, S. Jacinavičius, M. Brikas, S. Balickas: **Picosecond lasers in micromachining**, Proc. 22nd Int. Congress ICALEO 2003 (2003), pp.134-141.
- [17] Fundamental XPS data from pure elements, pure oxides, and chemical compounds. XPS International Inc. (1999)
- [18] A. Avila, I. Montero, L. Galan, J.M. Ripalda, R. Levy: **Behavior of oxygen doped SiC thin films: An x-ray photoelectron spectroscopy study**, J. Appl. Phys. **89**, 212 (2000)
- [19] C. Benndorf, B. Caus, H. Egert, F. Seidel: **Theime: Identification of Cu(I) and Cu(II) oxides by electron spectroscopic methods: AES, ELS and UPS investigations**. J. Electron. Spectrosc. Relat. Phenom **19**, 77 (1980)
- [20] Y.S. Tan, S.Y.M. Chooi, C.Y. Sin, P.Y. Ee, M.P. Srinivasan, S.O. Pehkonen: **Angled XPS analysis of low-k dielectric surfaces after cleaning**, Thin Solid Films **462–463**, 250 (2004)
- [21] H.Y. Zheng, A.R. Zareena, H. Huang: **Femtosecond laser processing of Nitinol**, STR/03/028/MT, pp. 1-6 (2004).

CURRICULUM VITAE

1. Name: Marijus
2. Surname: Brikas
3. Date of birth: 1981 08 07

4. Education:

1999m: Siauliai Ragaine secondary school.

2003m: Bachelor of Vilnius University, Physics Department, management of modern technologies.

2005m: Master of the Vilnius University, Physics Department, laser physics and optical technology degree program. Defended the work, „Laser micro-processing effects on properties of silicon“.

Since 2005: PhD studies at the Institute of Physics. Direction: laser microprocessing.

5. Work experience:

2003m: Vilnius University, Faculty of Physics, Department of Semiconductor Physics, the technician.

2003m – 2004m: UAB “EKSPLA” engineer - designer.

2004m: Institute of Physics, engineer.

2006m: Institute of Physics, a junior researcher. Current Employer.

6. Scientific activities:

2005-2011 m. Institute of Physics, PhD student (thesis prepared for consideration). Research direction is the laser interaction with metals and semiconductors and its application in materials processing. Improved qualifications at the Hanover Laser Center in 2006 and 2007. He is co-author of 15 articles in scientific journals and 30 presentations at international conferences.

Santrauka

Disertacijos tikslas yra ištirti didelio impulsų pasikartojimo dažnio pikosekundinių lazerių pritaikomumą medžiagų mikroapdirbimui, bei išaiškinti tokių lazerių spinduliuotės sąveikos su metalais ir siliciu ypatybes.

Eksperimentiškai buvo ištirta abliacijos slenkščio ir akumuliacijos koeficiento priklausomybė nuo lazerio impulso trukmės siliciui ir metalams. Medžiagą paveikus keletu lazerių impulsų, abliacijos slenkstis mažėja, nes kaupiasi ikiabliaciniai defektai. Akumuliaciniai efektai stipriau pasireiškia pikosekundiniams nei nanosekundiniams impulsams. Sukurtas ir eksperimentiškai patvirtintas modelis optimalioms fokusavimo sąlygoms surasti, siekiant maksimalios abliacijos spartos. Maksimalus lazerinės abliacijos našumas pasiekiamas, kai energijos tankis Gauso pluošto centre 7,4 karto viršija medžiagos abliacijos slenkstį. Didelei impulso energijai, medžiagos nugarinimo efektyvumas mažėja dėl ekranuojančio plazmos poveikio.

Įvairių impulso trukmių lazeriai buvo panaudoti silicio gręžimui bei pjovimui. Paviršiaus spektroskopijos metodais, nustatyta, kad pjovimo metu silicis yra legiruojamas anglimi iki 5 μm gylio iš atmosferoje esančio anglies dvideginio, o susidariusi silicio karbido fazė įtakoja lazerinio pjovimo kokybę silicio bandinio gylyje. Inertinė azoto aplinka gali apsaugoti nuo silicio paviršiaus karbonizavimosi.

Taikant didelio impulsų pasikartojimo dažnio pikosekundinius lazerius sudėtingos formos detalių gamybai, rasti sąryšiai tarp paviršiaus šiurkštumo bei proceso parametrų. Pikosekundiniai lazeriai buvo panaudoti, išpjaunant elektrostatinių mikropozicionieriaus struktūras iš silicio ir formuojant 3D išėmas įrankiniame pliene ir nitinolyje. Pjaunant lazeriu stentus iš Nitinolio, šilumos nukreipimas nuo ruošinio riboja galimą panaudoti lazerio vidutinę galią ir tuo pačiu pasiekiamą efektyvų pjovimo greitį.

Pikosekundiniu lazeriu galima efektyviai generuoti siauro dydžių skirstinio nanodaleles skysčiuose. Sidabro nanodalelių generavimo vandenyje sparta pasiekta 8,6 $\mu\text{g/s}$, esant 5,5 W vidutinei lazerio spinduliuotės galiai ir 50 kHz impulsų pasikartojimo dažniui. Aukso nanodalelės buvo generuojamos 5,9 $\mu\text{g/s}$ sparta n-heksano terpėje. Lazerinės abliacijos metodu pagamintos nanodalelės išlieka stabilios ilgą laiką.